RSC Advances

PAPER

View Article Online
View Journal | View Issue

Cite this: *RSC Adv.*, 2025, **15**, 12940

A low-ammonium consumption method for preparing high-purity V_2O_5 from vanadium-rich liquids with high impurity content

Bingjie Sun, [abcd] Jing Huang,*[abcd] Yimin Zhang[abcd] and Pengcheng Hu[abcd]

The conventional method for preparing V_2O_5 from vanadium-rich leachate suffers from three significant drawbacks: low purity, excessive ammonium consumption, and the generation of high-ammonia–nitrogen wastewater. To address these challenges, this study introduces an integrated process involving D2EHPA saponification extraction, hydrolysis vanadium precipitation, and ammonium purification for the production of high-purity V_2O_5 from high-impurity vanadium-rich liquid. After three-stage counter-current extraction at a 60% saponification degree, 40 vol% D2EHPA concentration, an initial pH of 1.8, a phase ratio (O/A) of 2 : 1, and an extraction time of 8 minutes, followed by three-stage counter-current stripping at 2 mol L^{-1} H_2SO_4 concentration, a phase ratio (O/A) of 2 : 1, and stripping time of 20 minutes, the concentrations of Fe^{2+} and Al^{3+} in the stripping solution were 0.034 g L^{-1} and 0.439 g L^{-1}, respectively. These contaminants were effectively eliminated with removal efficiencies of 98.78% and 97.93%. At an ammonium addition coefficient of 1, V_2O_5 was prepared with 99.9% purity using the hydrolysis vanadium precipitation-ammonium salt purification approach, which consumed 83% less ammonium salt compared to the ammonium precipitation method. This study significantly reduces ammonium salt usage and provides a scalable, environmentally friendly process for high-purity V_2O_5 production.

Received 14th March 2025
Accepted 15th April 2025

DOI: 10.1039/d5ra01838b

rsc.li/rsc-advances

1. Introduction

Vanadium is a strategic metal with significant importance in high-tech industries due to its unique chemical and physical properties.[1–3] V_2O_5, a key vanadium oxide, is widely used in catalysts, nanomaterials, and pharmaceuticals, and in the chemical and metallurgical industries.[4–7] The demand for high-purity V_2O_5 has particularly increased due to its application in vanadium redox flow batteries.[8] Consequently, research on the preparation of high-purity V_2O_5 has garnered substantial interest.[9]

The vanadium-containing leachate produced through acid leaching of vanadium shale contains a significant amount of impurities. Therefore, vanadium products require extensive purification and enrichment to remove these impurities before further processing.[10,11] However, even after purification, the vanadium-rich liquid still contains substantial levels of impurity ions, which directly affect the purity of the resulting V_2O_5 products.[12] Impurities such as Fe, Al, Ca, and P can significantly decrease vanadium precipitation efficiency and the purity of V_2O_5 in ammonium salt precipitation processes.[13] Thus, to produce high-purity V_2O_5, vanadium-rich liquids must undergo significant impurity removal before precipitation.

C. Chao *et al.*[14] employed hydrolysis vanadium precipitation to obtain red vanadium, followed by alkali solubilization, flocculant removal, and ammonium vanadium precipitation to prepare high-purity V_2O_5. However, this method leads to high vanadium losses, excessive ammonium consumption, and the production of a large volume of ammonia–nitrogen wastewater, which poses an environmental threat. Therefore, there is a pressing need for an environmentally friendly technique that minimizes vanadium losses. Solvent extraction is an effective method for separating vanadium from impurities due to its efficiency, cost-effectiveness, and ease of implementation.[15,16] Li W. *et al.*[17] demonstrated that solvent extraction outperforms ion exchange in removing impurities from vanadium-rich solutions while maximizing vanadium recovery. Among various extractants, Di-(2-ethylhexyl) phosphoric acid (D2EHPA) has become a widely used extractant due to its superior performance in acidic solutions.[18–20] D2EHPA is an acidic extractant, which can displace a large amount of H^+ in the extraction process and reduce the extraction rate. After saponification, H^+ in D2EHPA is replaced by Na^+ or K^+ in the

[a]School of Resource and Environmental Engineering, Wuhan University of Science and Technology, Wuhan, Hubei 430081, China. E-mail: crystal208@126.com
[b]State Environmental Protection Key Laboratory of Mineral Metallurgical Resources Utilization and Pollution Control, Wuhan, Hubei 430081, China
[c]Collaborative Innovation Center of Strategic Vanadium Resources Utilization, Wuhan, Hubei 430081, China
[d]Hubei Provincial Engineering Technology Research Center of High Efficient Cleaning Utilization for Shale Vanadium Resource, Wuhan 430081, China

saponification agent, and the content of H^+ released during extraction is reduced, and the dimer of D2EHPA is dissociated into haploid after saponification, which greatly improves the extraction rate.[21]

The vanadium precipitation process is a critical step in vanadium recovery from vanadium shale and other vanadium-bearing deposits.[22,23] In recent years, acidic ammonium precipitation has been widely used in industrial production due to its high precipitation efficiency and excellent purity of vanadium products.[24–26] However, this method consumes large amounts of ammonium salt and produces substantial volumes of ammonia nitrogen wastewater.[27,28] Although hydrolysis vanadium precipitation results in lower-purity vanadium products (approximately 85.00%), it is highly efficient, does not generate ammonia–nitrogen wastewater, and is less environmentally damaging.[29,30] As environmental protection regulations tighten, the conventional vanadium precipitation process, which uses excessive ammonium salt and produces low-quality products, has hindered the future development of vanadium extraction technologies.

Polyvanadate ions preferentially form alkali metal salts in the order of $K^+ > NH_4^+ > Na^+ > H^+$.[31] Based on this principle, high-purity V_2O_5 products can be generated through hydrolysis vanadium precipitation and ammonium salt purification. In this approach, sodium polyvanadate is first prepared through hydrolysis vanadium precipitation and then purified with an ammonium salt solution. Polyvanadate ions exhibit a stronger affinity for NH_4^+ than Na^+, enabling NH_4^+ to replace Na^+ in sodium polyvanadate to form ammonium polyvanadate,[32] which enhances the purity of the final V_2O_5 product. This method effectively reduces ammonium consumption while achieving high-purity V_2O_5.

This study aims to develop a high-purity V_2O_5 preparation process with efficient impurity removal and low ammonium consumption. The process involves D2EHPA saponification extraction for impurity removal, hydrolysis vanadium precipitation to form sodium polyvanadate, and ammonium salt purification to yield high-purity V_2O_5. The proposed method offers excellent impurity removal, reduced ammonium consumption, and environmental sustainability, making it a promising approach for the future of the vanadium extraction industry.

2. Materials and methods

2.1. Materials

In this study, vanadium-rich liquid produced by a vanadium factory in Shaanxi province is used as a raw material. The primary impurity ions in the vanadium-rich liquid used in this study are Fe^{2+} and Al^{3+} (Table 1). All solutions were prepared using deionized water, and all reagents were of analytical grade.

Table 1 Composition of vanadium-rich liquid (g L^{-1})

Element	V	Fe	Al	Zn	Na	K	Mg	P
Content	54.23	2.78	21.21	3.88	0.707	0.545	0.304	0.36

D2EHPA was for the extraction of vanadium, with NaOH as the saponification agent, $NaClO_3$ to oxidize V(IV) to V(V), Na_2CO_3 and H_2SO_4 to adjust pH, and NH_4Cl for washing. The initial pH of the vanadium-rich solution was −0.4, determined using a pH meter (S-3, Shanghai Lida Instrument Factory, China).

2.2. Experimental steps

The high-purity V_2O_5 products were prepared through the D2EHPA saponification extraction-hydrolysis vanadium precipitation-ammonium salt purification approach, as outlined in Fig. 1. The vanadium-rich liquid used in step 1 is a simulated vanadium-rich liquid configured according to the composition shown in Table 1.

2.2.1. Impurities elimination process. Fe^{2+}, Al^{3+}, and other impurity ions in the vanadium-rich liquid must be removed before hydrolysis vanadium precipitation. To establish acceptable Fe^{2+} and Al^{3+} concentrations that meet the YB/T 5304-2017 standard, the effects of Fe^{2+} and Al^{3+} concentration on the purity of the vanadium precipitation products were investigated.

D2EHPA saponification extraction was applied to remove impurity ions and produce high-purity V_2O_5. The saponification agent was added to the organic phase (mixture of D2EHPA and sulfonated kerosene) and stirred until clear. The saponification degree was calculated using eqn (1),[33] extraction percentage(E), stripping percentage (S), partition ratio (D) and separation factor ($\beta_{M1/M2}$) were calculated from eqn (2)–(5).

$$\text{Saponification degree} = \frac{n(\text{NaOH})}{n(\text{D2EHPA})} \times 100\% \quad (1)$$

$$E = \left(1 - \frac{C_R V_R}{C_F V_F}\right) \times 100\% \quad (2)$$

$$S = \frac{C_S V_S}{C_F V_F - C_R V_R} \times 100\% \quad (3)$$

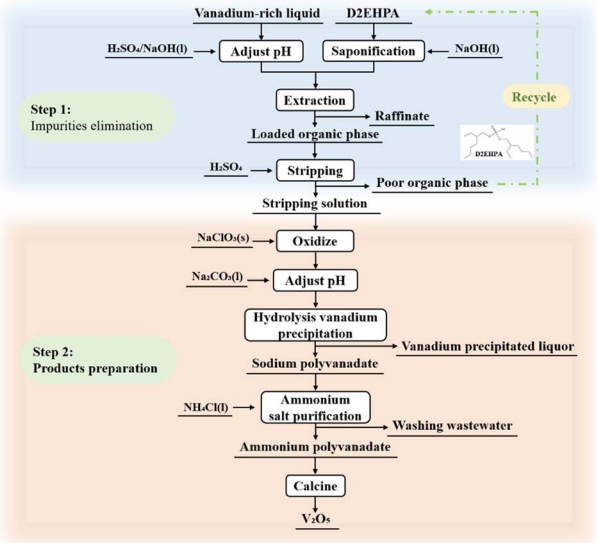

Fig. 1 A flowchart of the V_2O_5 preparation process.

$$D = \frac{C_{org}}{C_R} \quad (4)$$

$$\beta_{M1/M2} = \frac{D_{M1}}{D_{M2}} \quad (5)$$

where C_F, C_R, C_S, and C_{org} represent the metal concentrations (g L^{-1}) in the feed solution (vanadium-rich liquid), raffinate, stripping solution, and organic phase, respectively; V_F, V_R, and V_S represent the volumes (L) of the feed solution, raffinate, and stripping solution, respectively; and M1 and M2 represent the metal elements.

2.2.2. Hydrolysis vanadium precipitation-ammonium salt purification. Different experimental influencing factors were investigated to establish the optimum parameters for hydrolysis vanadium precipitation-ammonium salt purification. Each experiment was conducted by magnetic stirring in a thermostatic water bath. First, $NaClO_3$ was applied to oxidize the vanadium-rich liquid's V(IV) and Fe^{2+} to V(V) and Fe^{3+}. Second, Na_2CO_3 was added to adjust the liquid's pH, the pH-adjusted solution was then heated and stirred for a period. Eventually, solid–liquid separation formed the sodium polyvanadate and vanadium precipitation liquor. The ammonium polyvanadate was produced by incorporating 2% NH_4Cl solution and stirring. The dried vanadium precipitate was then calcined at 500–550 °C for 30–60 min to produce V_2O_5. Eventually, solid–liquid separation formed the precipitation fluid of vanadium and sodium polyvanadate. The ammonium polyvanadate was produced by incorporating 2% NH_4Cl solution with sodium polyvanadate and stirring. Using the ammonium ferrous sulfate titration method, the concentration of vanadium in the vanadium precipitated liquor and washing wastewater was calculated. In addition, the percentage of vanadium precipitation and vanadium loss were computed. The vanadium precipitation percentage (η), vanadium loss (L), and ammonium addition coefficient (K) were determined using eqn (6)–(8).

$$\eta = 1 - \frac{C_b V_b}{C_a V_a} \times 100\% \quad (6)$$

$$L = \frac{C_c V_c}{C_a V_a} \times 100\% \quad (7)$$

$$K = \frac{n(NH_4^+)}{n(V_2O_5)} \quad (8)$$

where C_a, C_b, and C_c are the vanadium concentration (g L^{-1}) in vanadium-rich liquid, washing wastewater, and vanadium precipitated liquor, respectively; V_a, V_b, and V_c are the volume (L) of vanadium-rich liquid, washing wastewater, and vanadium precipitated liquor, respectively; n (NH_4^+) is the number of ammonium ions in the ammonium salt solution and n (V_2O_5) is the amount of vanadium in the vanadium-rich solution.

2.3. Analysis methods

Ammonium ferrous sulfate titration was used to determine the concentration of vanadium in solution (GB/T 8704.5-2020). The V_2O_5 products' elemental content and the ionic content in solution were determined using an inductively coupled plasma optical emission spectrometer (ICP-OES; Thermo Elemental, USA). The physical composition of vanadium-containing products was determined using X-ray diffraction (XRD; Rigaku, Japan). The vanadium-containing products' microstructures and corresponding elemental distributions were examined using a field emission scanning electron microscope (ESEM; Quattro S, USA) equipped with an energy-dispersive spectrometer (EDS; BRUKER, Germany). The content of crystal water in vanadium precipitation products was determined using thermogravimetric (TG; Netzsch, Selb, Germany). To document the changes in chemical bonding throughout the reaction, Fourier transform infrared (FTIR) spectra (Thermo Fisher Scientific Co., MA, USA) were employed. The purity of V_2O_5 products was determined according to the standard YB/T 5304-2017.

3. Results and discussion

3.1. Impurities elimination process

3.1.1. Effect of Fe^{2+} and Al^{3+} on V_2O_5 purity. To avoid interference from other impurities, a vanadium-rich liquid free of impurity ions was prepared, and different concentrations of Fe^{2+} and Al^{3+} were added. The effects of Fe^{2+} and Al^{3+} concentration on the purity of the V_2O_5 product were analyzed (Fig. 2).

Fig. 2(b) demonstrates that the Al^{3+} concentration has a minimal effect on the purity of V_2O_5. Specifically, as the Al^{3+} concentration increased from 5 g L^{-1} to 25 g L^{-1}, the purity of V_2O_5 decreased slightly from 99.98% to 99.96%, while the aluminum content increased from 0.0007 wt% to 0.001 wt%. Fig. 2(a) indicates that the iron content in V_2O_5 products increased with the rise in Fe^{2+} concentration in the vanadium-rich liquid. When the Fe^{2+} concentration was 0.2 g L^{-1}, the iron content in the V_2O_5 products was 0.082 wt%, whereas at a Fe^{2+} concentration of 1 g L^{-1}, the iron content increased to 0.276 wt%. The purity of the V_2O_5 products meets the V_2O_5 98-P standard outlined in the YB/T 5304-2017 specification when the Fe^{2+} concentration in the vanadium-rich solution is less than 0.2 g L^{-1}. Therefore, considering various iron removal methods, D2EHPA extraction was chosen as the optimal process for eliminating iron and producing high-purity V_2O_5 products that meet the required standard.

3.1.2. Extraction process. The vanadium-rich liquid used in this study exhibited a high vanadium concentration. Direct extraction led to a significant decrease in the pH of the aqueous phase due to the displacement of vanadium and hydrogen ions by D2EHPA, resulting in a low extraction rate.[34] By employing NaOH as a saponifier, sodium ions replace the hydrogen ions in D2EHPA during the saponification process, leading to a lower pH in the aqueous phase, which facilitates the smooth progression of the extraction reaction.[35] The impact of the saponification degree of D2EHPA on vanadium extraction was examined under the following conditions: an initial pH of 1.8, a D2EHPA concentration of 40 vol%, a phase ratio (O/A) of 2 : 1, and an extraction time of 8 minutes.

As shown in Fig. 3, the vanadium extraction percentage increased from 55.93% to 89.11%, while the Fe^{2+} extraction percentage increased from 13.61% to 24.66% as the

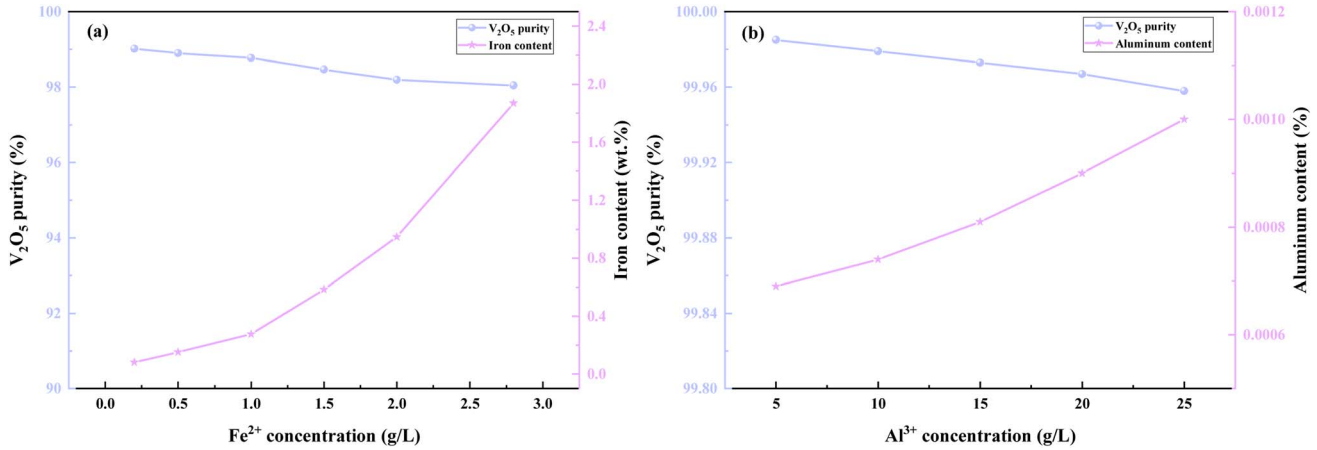

Fig. 2 Effect of (a) Fe^{2+} and (b) Al^{3+} concentration on V_2O_5 purity (vanadium precipitation conditions: initial pH 1.8, temperature 95 °C, time 1.5 h).

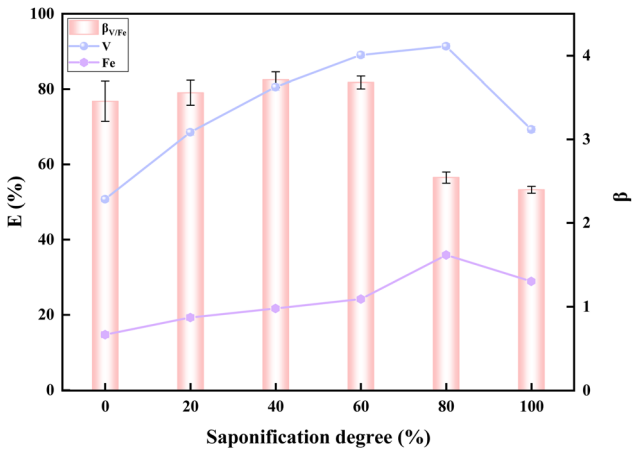

Fig. 3 Effect of saponification degree on extraction.

saponification degree of D2EHPA was raised from 0% to 60%. However, no significant increase in vanadium extraction was observed as the saponification degree increased from 60% to 80%, whereas the Fe^{2+} extraction percentage rose from 24.66% to 35.91%. When the saponification degree was increased from 80% to 100%, the vanadium extracted proportion dropped to 70.08%. Therefore, a saponification degree of 60% was determined to be optimal for achieving high vanadium recovery and effective vanadium–iron separation.

The effects of initial pH, D2EHPA concentration, phase ratio (O/A), and extraction time on the vanadium extraction and vanadium–iron separation were further investigated under the optimal saponification degree of 60%, as presented in Fig. 4.

The impact of initial pH on vanadium extraction was assessed at an extraction time of 8 minutes, D2EHPA concentration of 40 vol%, and phase ratio (O/A) of 2 : 1. Fig. 4(a) illustrates that the vanadium extraction rate increased significantly from 55.64% to 89.15% as the initial pH of the feed solution was raised from 0.4 to 1.8. The vanadium extraction rate remained constant beyond this pH range. Similarly, the Fe^{2+} extraction rate increased steadily as the pH increased. The optimal vanadium extraction rate and vanadium–iron separation coefficient were observed at an initial pH of 1.8, which was thus selected as the optimal pH.

D2EHPA concentration and phase ratio are critical factors influencing vanadium recovery and vanadium–iron separation. Given the high vanadium concentration in the vanadium-rich liquid, the extractant dosage plays a significant role in vanadium recovery. The effect of D2EHPA concentration was examined at an initial pH of 1.8, a phase ratio (O/A) of 2 : 1, and an extraction time of 8 minutes. The results in Fig. 4(b) indicate that the vanadium extraction rate increased from 15.35% to 92.59%, while the Fe^{2+} extraction rate increased from 12.55% to 30.19% as the D2EHPA concentration was raised from 10 vol% to 50 vol%. Considering both vanadium recovery and vanadium–iron separation, a D2EHPA concentration of 40 vol% was selected as optimal.

The effect of phase ratio (O/A) on vanadium extraction was studied at an initial pH of 1.8, a D2EHPA concentration of 40 vol%, and an extraction time of 8 minutes. As shown in Fig. 4(c), the extraction rates of vanadium and Fe^{2+} increased from 9.79% to 98.36% and from 6.69% to 46.16%, respectively, as the phase ratio (O/A) was adjusted from 1 : 2 to 3 : 1. While a higher phase ratio improved vanadium recovery, the vanadium–iron separation effect diminished. The optimal phase ratio (O/A) for maximizing vanadium–iron separation, with a vanadium extraction rate of 89.65%, was determined to be 2 : 1.

The impact of extraction time on vanadium extraction was investigated at an initial pH of 1.8, D2EHPA concentration of 40 vol%, and a phase ratio (O/A) of 2 : 1. Fig. 4(d) shows that the vanadium extraction rate increased from 74.09% to 87.31% as the extraction time was extended from 2 to 6 minutes, with the extraction rate stabilizing after 8 minutes. The vanadium–iron separation coefficient remained unchanged with longer extraction times. Thus, an extraction time of 6 minutes was identified as optimal.

The McCabe–Thiele diagram for vanadium concentrations in the aqueous and organic phases under optimal conditions

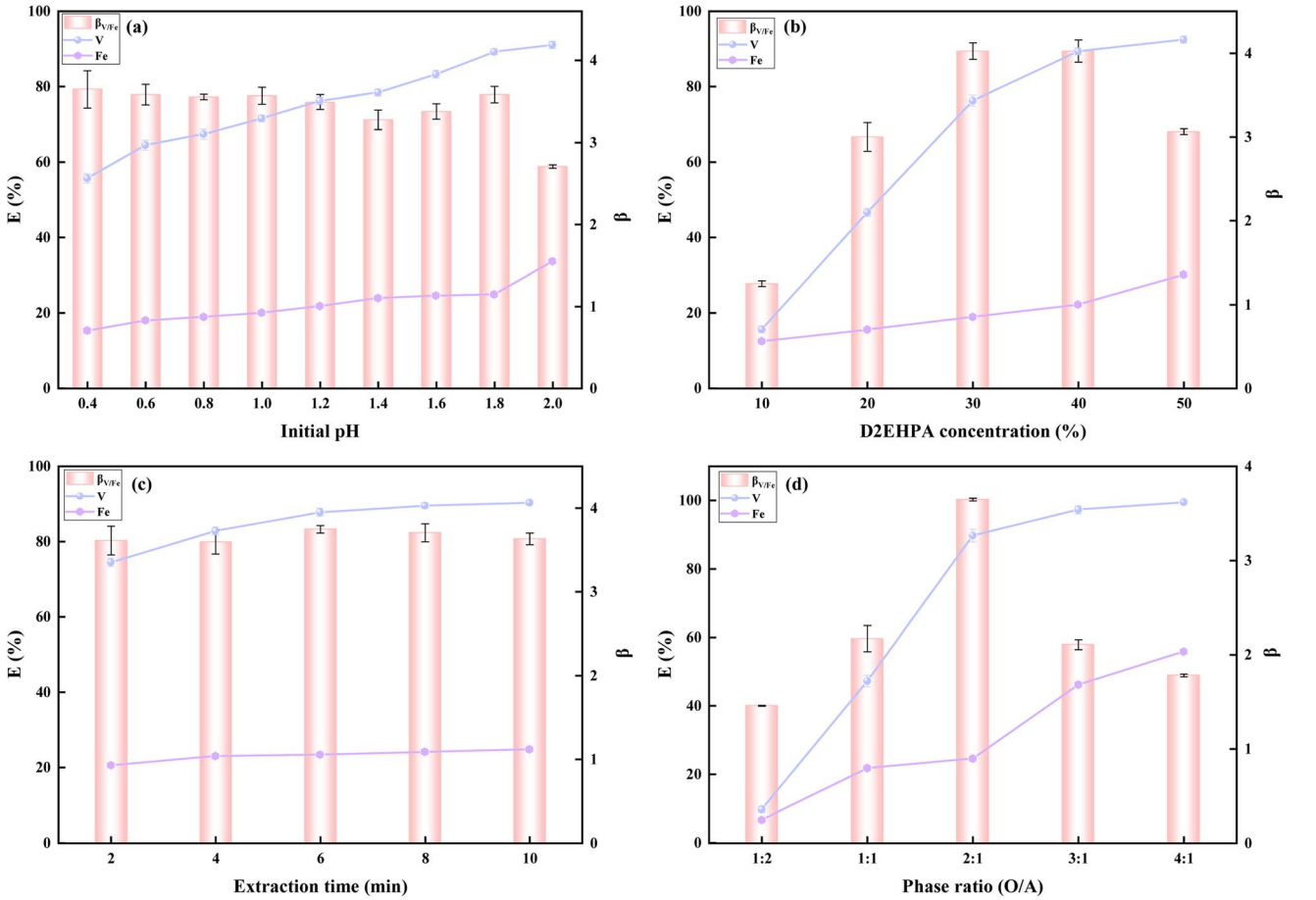

Fig. 4 Effect of initial pH (a), D2EHPA concentration (b), phase ratio (O/A) (c), and extraction time (d) on the extraction rate of vanadium and Fe^{2+} and $\beta_{V/Fe}$.

(pH of 1.8, D2EHPA concentration of 40%, and extraction time of 8 minutes) was plotted, as shown in Fig. 5. The phase ratio (O/A) was set to 2 : 1. Theoretically, the vanadium concentration in the raffinate can be reduced to 50 mg L^{-1} after two-stage counter-current extraction. However, three-stage counter-current extraction was performed in practice to achieve the optimal experimental parameters. The vanadium extraction rate reached 99%, with vanadium and Fe^{2+} concentrations in the loaded organic phase of 26.84 g L^{-1} and 0.88 g L^{-1}, respectively.

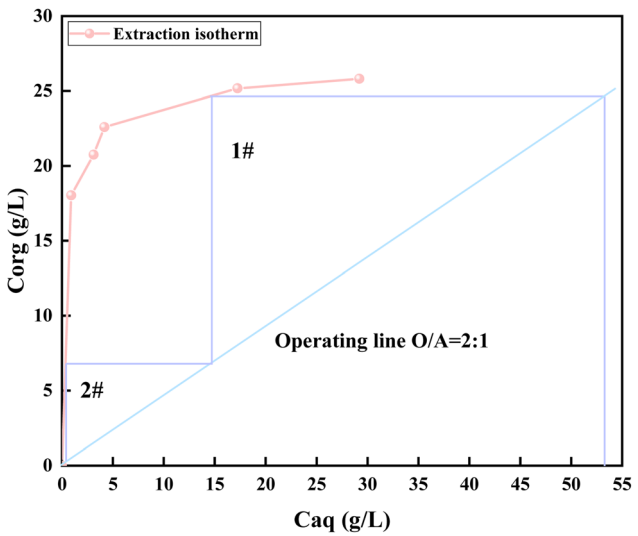

Fig. 5 McCabe–Thiele diagram for determining the number of vanadium extraction stages (conditions: initial pH of 1.8, D2EHPA concentration of 40 vol%, time of 8 minutes).

3.1.3. Stripping process. The concentration of Fe^{2+} in the stripping solution is directly linked to the purity of V_2O_5 products. As the extraction process removes most impurity ions and the vanadium concentration in the feed solution meets the requirement for hydrolysis vanadium precipitation, the stripping process must ensure effective vanadium recovery while minimizing the entry of Fe^{2+} into the stripping solution. The impacts of phase ratio (O/A), H_2SO_4 concentration, and stripping time on vanadium and Fe^{2+} stripping rates, as well as the vanadium–iron separation coefficient, were evaluated, as shown in Fig. 6.

The phase ratio (O/A) determines the vanadium concentration in the stripping solution. The effect of phase ratio was investigated at an H_2SO_4 concentration of 2 mol L^{-1} and a stripping time of 30 minutes. As shown in Fig. 6(a), the vanadium stripping rate decreased significantly, and the vanadium–iron separation coefficient continuously declined as the phase ratio increased. At a phase ratio of 2 : 1, the vanadium

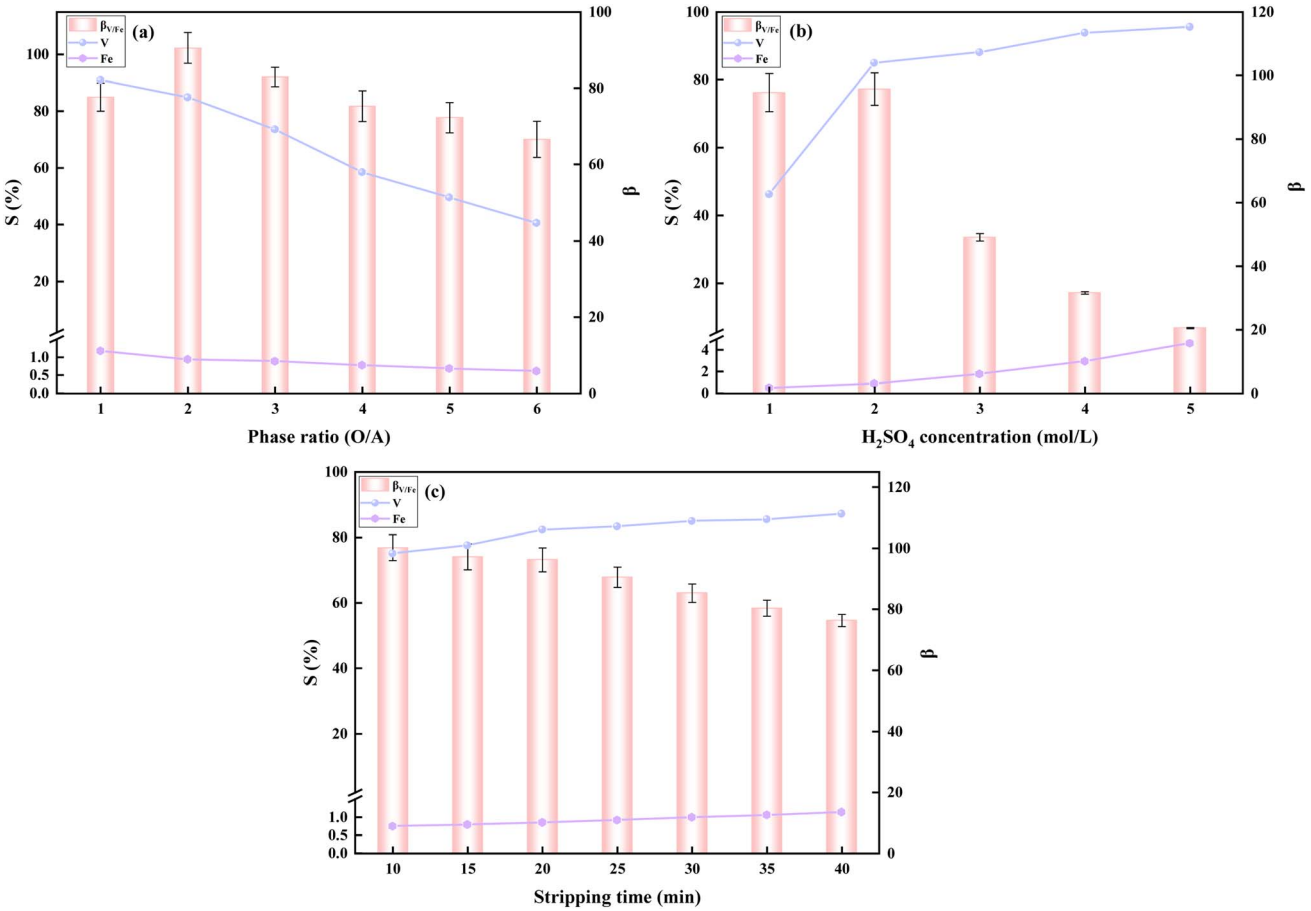

Fig. 6 Effect of phase ratio (a), H_2SO_4 concentration (b), and time (c) on vanadium and Fe^{2+} stripping rates and $\beta_{V/Fe}$.

extraction rate was 84.95%, and the vanadium–iron separation coefficient was 91.15. Since the aim of this investigation was not to further concentrate vanadium, the optimum phase ratio (O/A) was determined to be 2 : 1.

The effect of H_2SO_4 concentration, ranging from 1 to 4 mol L^{-1}, was examined at a stripping time of 30 minutes and a phase ratio of 2 : 1. The results, shown in Fig. 6(b), indicate a sharp increase in vanadium stripping rate from 46.14% to 84.95% as the H_2SO_4 concentration was raised from 1 mol L^{-1} to 2 mol L^{-1}. Further increasing the H_2SO_4 concentration to 4 mol L^{-1} raised the vanadium stripping rate to 93.76%, but the vanadium–iron separation coefficient decreased significantly. Considering the impact of Fe^{2+} concentration on the purity of the V_2O_5 products, the optimal H_2SO_4 concentration was selected as 2 mol L^{-1}.

The effect of stripping time was studied at an H_2SO_4 concentration of 2 mol L^{-1} and a phase ratio (O/A) of 2 : 1. As shown in Fig. 6(c), from 10 minutes to 20 minutes, the vanadium stripping rate increased from 75.02% to 82.22%, continuing to rise with longer stripping times. However, with extended stripping time, the vanadium–iron separation coefficient decreased, and the vanadium stripping rate reached a plateau. Therefore, the optimal stripping time was determined to be 20 minutes.

The McCabe–Thiele diagram was constructed based on the optimal stripping conditions (H_2SO_4 concentration of 2 mol L^{-1} and stripping time of 20 minutes). As depicted in Fig. 7, the vanadium concentration in the raffinate phase was reduced to 30 mg L^{-1} after two-stage counter-current stripping. In practice, a three-stage counter-current stripping process was employed to achieve the optimal experimental parameters, with the vanadium stripping rate reaching 99.8%. The main components of the stripping solution are shown in Table 2, where the concentrations of vanadium and Fe^{2+} were 53.57 g L^{-1} and 0.034 g L^{-1}, respectively.

3.1.4. D2EHPA saponification extraction mechanism. To investigate the saponification extraction mechanism of D2EHPA, FTIR analysis was carried out on fresh, saponified, loaded, and poor organic phases. The results are shown in Fig. 8.

In the unsaponified D2EHPA organic phase, the molecules form strong hydrogen bonds with each other, predominantly as dimers.[36] As shown in Fig. 8, the P–O–H bond vibration peak at 2731 cm^{-1} in the fresh organic phase is hydrogen-bonded. In contrast, the P–O–H vibration peak in the saponified organic phase is significantly weakened, suggesting that some hydroxyl groups have been broken, with sodium ions replacing hydrogen ions. The P═O absorption peak at 1230 cm^{-1} in the loaded

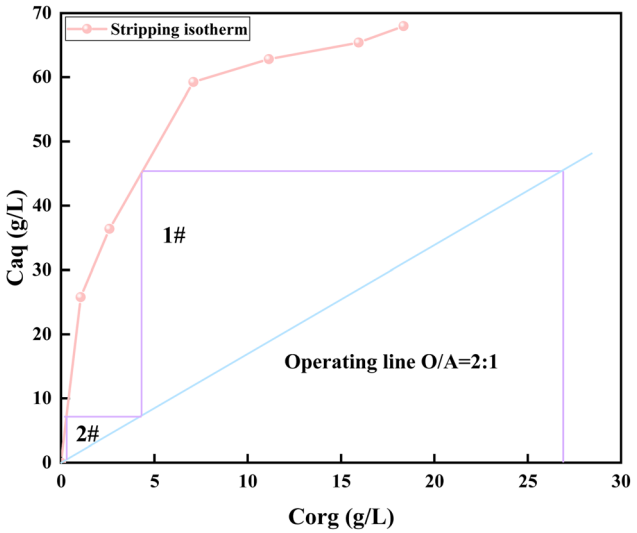

Fig. 7 McCabe–Thiele diagram for determining the number of vanadium stripping stages (conditions: H_2SO_4 concentration of 2 mol L^{-1}, stripping time of 8 minutes).

Table 2 Composition of stripping solution (g L^{-1})

Element	V	Fe	Al	Zn	Na	K	Mg	P
Content	53.57	0.034	0.439	0.185	0.017	0.004	0.014	0.012

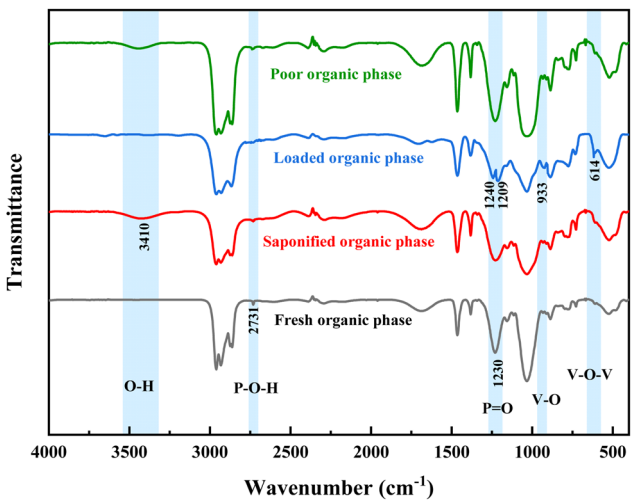

Fig. 8 FTIR spectra of organic phases.

organic phase splits into two distinct P═O peaks at 1209 cm^{-1} and 1240 cm^{-1}. Additionally, the absorption peaks at 933 cm^{-1} and 614 cm^{-1} correspond to the V–O and V–O–V bonds, respectively, indicating that vanadium is transferred from the aqueous phase into the organic phase during extraction. The O–H bond stretching vibration peaks at 3410 cm^{-1} in both the saponified organic and raffinate phases, suggesting the incorporation of water molecules into the organic phase during saponification. The spectra of the raffinate and fresh organic phases are similar, and the disappearance of the V–O–V and V–O peaks following sulfuric acid stripping, alongside the recovery of the P═O peaks, indicates that the organic phase can be regenerated and reused.

3.2. Hydrolysis vanadium precipitation-ammonium salt purification

3.2.1. Hydrolysis vanadium precipitation process. This study investigated the key parameters (pH, reaction time, and temperature) influencing the hydrolysis vanadium precipitation process. The experimental results are presented in Fig. 9.

The effect of initial pH on the hydrolysis vanadium precipitation was examined at a reaction time of 2 hours and a temperature of 98 °C. As shown in Fig. 9(a), the vanadium precipitation rate increased consistently with the rise in initial pH. The precipitation rate reached 99.22% when the initial pH was 1.8, and no further increase in precipitation rate was observed for pH values above 1.8. Therefore, the optimal initial pH was determined to be 1.8.

The effect of reaction time on hydrolysis vanadium precipitation was evaluated at an initial pH of 1.8 and a temperature of 98 °C. As depicted in Fig. 9(b), the vanadium precipitation rate increased progressively with longer reaction times. The rate reached 99.20% after 1.5 hours, and no significant change in the precipitation rate was observed beyond this time. To optimize energy usage and manufacturing efficiency, the optimal reaction time was determined to be 1.5 hours.

The effect of reaction temperature on hydrolysis vanadium precipitation was studied at an initial pH of 1.8 and a reaction time of 1.5 hours. As shown in Fig. 9(c), the vanadium precipitation rate increased with temperature, reaching a maximum of 99.13% at 95 °C. Further temperature increases did not lead to any additional improvement in precipitation. Consequently, the optimal reaction temperature was selected to be 95 °C.

The main parameters of the hydrolysis vanadium precipitation process were optimized to ensure the complete precipitation of vanadium from the vanadium-rich solution while minimizing vanadium loss during the process. As illustrated in Fig. 9, the vanadium precipitation rate reached 99.13% under the optimal conditions: an initial pH of 1.8, a reaction time of 1.5 hours, and a temperature of 95 °C.

3.2.2. Ammonium salt purification process. NH_4^+ exhibit a stronger binding affinity for vanadate ions to vanadate ions compared to Na^+, enabling the purification of the hydrolysis vanadium precipitation product using an ammonium salt solution to produce high-purity V_2O_5. In this study, NH_4Cl solution was used as the purification agent. The effects of the ammonium addition coefficient, purification temperature, purification time, and purification frequency on the purity of V_2O_5 were investigated, with the experimental results shown in Fig. 10.

The effect of the ammonium addition coefficient on purity was examined at a purification temperature of 25 °C, a purification time of 20 min, and a purification frequency of 1. As shown in Fig. 10(a), the purity of V_2O_5 increased significantly as the ammonium addition coefficient was increased from 0 to 1.

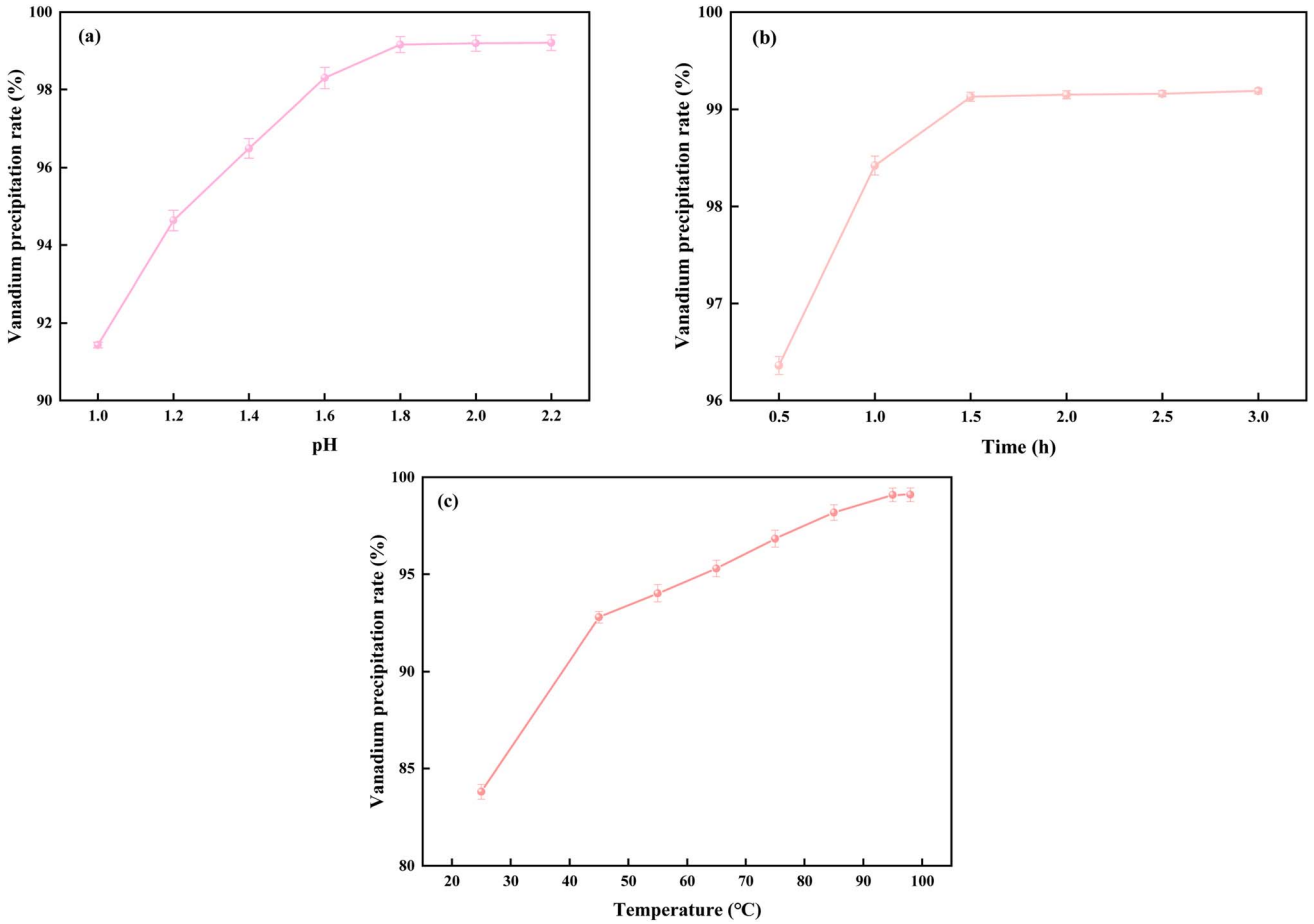

Fig. 9 Effect of initial pH (a), reaction time (b), and temperature (c) on vanadium precipitation rate.

However, as the ammonium addition coefficient continued to increase, the purity of V_2O_5 stabilized, while the vanadium loss rate increased. Therefore, the optimum ammonium addition coefficient was determined to be 1, balancing V_2O_5 purity improvement with reduced ammonium usage and vanadium loss.

The effect of purification temperature on purity was studied at an ammonium addition coefficient of 1, a purification time of 20 min, and a purification frequency of 1. The results, shown in Fig. 10(b), indicate that V_2O_5 purity gradually increased with the rise in temperature from 25 °C to 55 °C. However, further temperature increases led to a decline in purity and an increase in vanadium loss. Hence, the optimal purification temperature was determined to be 55 °C.

The effect of purification time on purity was investigated at an ammonium addition coefficient of 1, a purification temperature of 55 °C, and a purification frequency of 1. As shown in Fig. 10(c), the purity of V_2O_5 improved as the purification time was extended from 0 to 15 minutes. Beyond 15 minutes, the purity remained constant, while vanadium loss increased. Therefore, the optimal purification time was chosen to be 15 minutes.

The effect of purification frequency on V_2O_5 purity was studied at an ammonium addition coefficient of 1, a purification temperature of 55 °C, and a purification time of 15 minutes. As illustrated in Fig. 10(d), with the total ammonium consumption kept constant, the purity of V_2O_5 increased as the purification frequency was raised from 0 to 2. However, the purity remained unchanged when the purification frequency exceeded 2, indicating that the system had reached equilibrium. To ensure optimal V_2O_5 purity while enhancing manufacturing efficiency and reducing energy consumption, the optimal purification frequency was selected to be 2.

To assess the reduction in ammonium consumption, the hydrolysis vanadium precipitation-ammonium salt purification process was compared with the ammonium salt vanadium precipitation process. Ammonium salt (NH_4Cl) vanadium precipitation experiments were conducted on the solution obtained after D2EHPA saponification extraction, using an initial pH of 1.8, a temperature of 95 °C, and a reaction time of 1.5 hours. The results of these experiments are presented in Fig. 11.

As shown in Fig. 11, both the vanadium precipitation rate and purity increased with the ammonium addition coefficient. When the ammonium addition coefficient increased from 1 to 6, the vanadium precipitation rate increased from 98.33% to 99.43%, while the purity rose from 93.51% to 99.23%. When the ammonium addition coefficient exceeded 6, both the precipitation rate and purity remained constant. Therefore, the

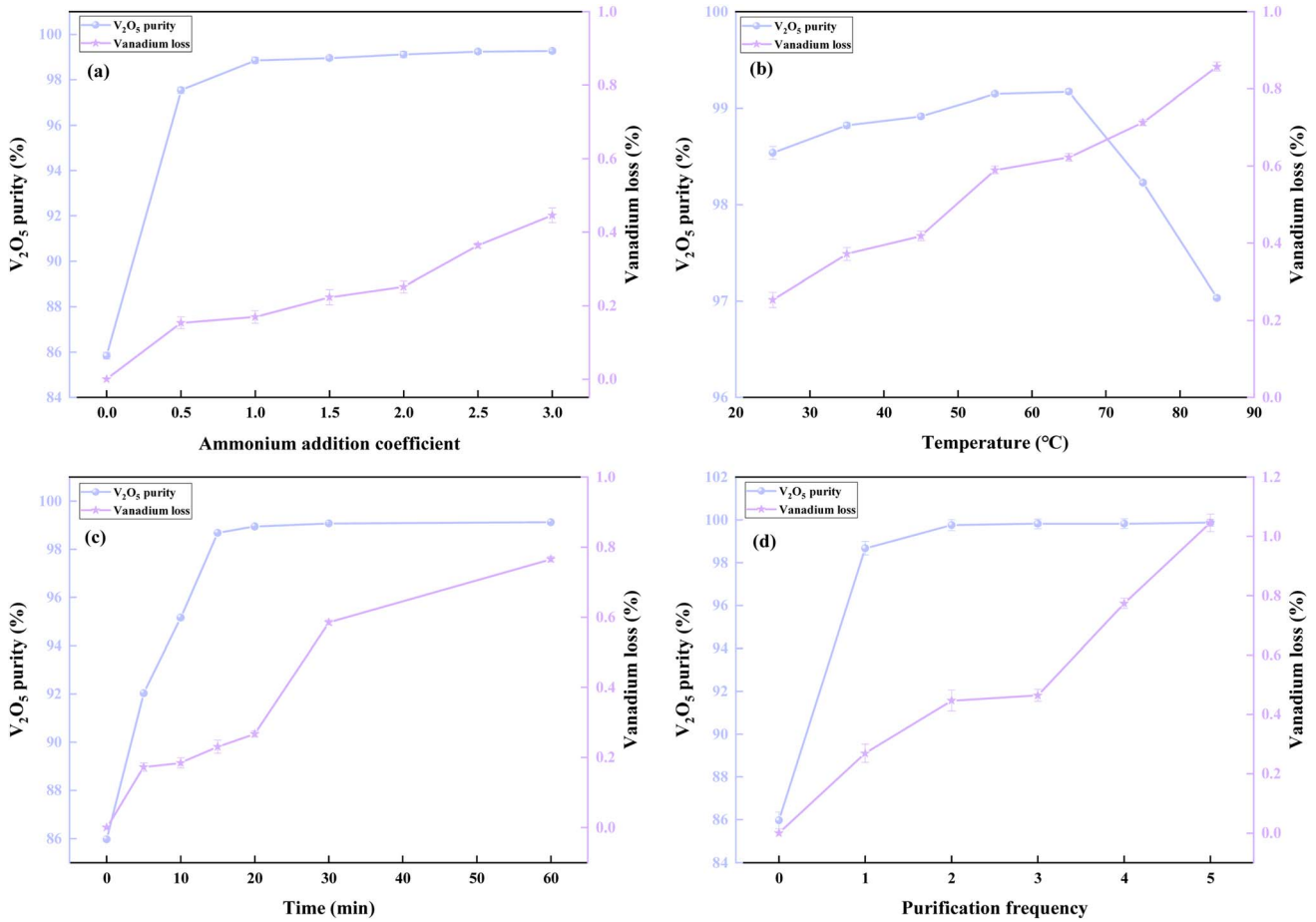

Fig. 10 Effect of ammonium addition coefficient (a), temperature (b), time (c), and purification frequency (d) on purity.

optimal ammonium addition coefficient for vanadium precipitation was selected to be 6.

The above experimental results demonstrate that the hydrolysis vanadium precipitation-ammonium salt purification process can significantly reduce the ammonium addition coefficient from 6 to 1, resulting in an 83% reduction in ammonium consumption compared to the conventional ammonium salt vanadium precipitation process. This makes the process more efficient and environmentally friendly for the production of high-purity V_2O_5.

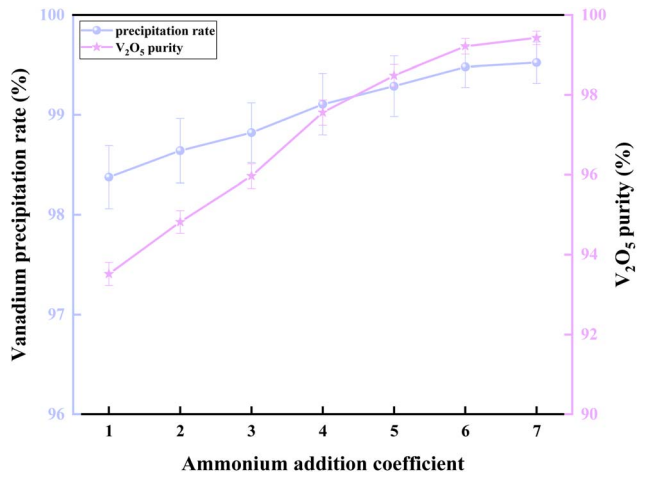

Fig. 11 Effect of ammonium addition coefficient on vanadium precipitation rate and purity.

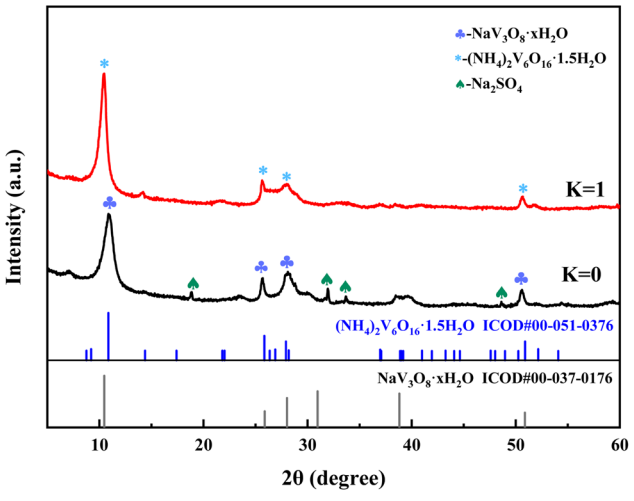

Fig. 12 XRD patterns of the hydrolysis vanadium precipitation product ($K = 0$) and ammonium salt purification product ($K = 1$).

3.2.3. Mechanisms analysis of ammonium salt purification. To explore the mechanisms underlying the ammonium salt purification process, the hydrolysis vanadium precipitation and ammonium salt purification products, prepared under optimal conditions, were analyzed using XRD and ESEM-EDS. These analyses aimed to identify changes in the physical phases of sodium polyvanadate and ammonium polyvanadate.

Fig. 12 shows the XRD patterns of both the hydrolysis vanadium precipitation and ammonium salt purification products. It can be observed that the $NaV_3O_8 \cdot xH_2O$ and Na_2SO_4 phases present in the hydrolysis vanadium precipitation product gradually disappear during the ammonium salt purification process. Concurrently, the formation of the $(NH_4)_2V_6O_{16} \cdot 1.5H_2O$ phase is evident. This suggests that NH_4^+ in the ammonium salt solution substitutes Na^+ in the hydrolysis vanadium precipitation product. In the XRD spectrum of the ammonium salt purification product, only the $(NH_4)_2V_6O_{16} \cdot 1.5H_2O$ phase is observed, confirming the low impurity content and the high purity of the resulting $(NH_4)_2V_6O_{16} \cdot 1.5H_2O$.

Fig. 13 and 14 reveal that the morphologies of both the hydrolysis vanadium precipitation and ammonium salt purification products are similar, exhibiting an irregular, layered structure. These observations suggest that the purification procedure does not significantly alter the microscopic morphology of the product. In Fig. 13, the hydrolysis vanadium precipitation product shows a strong correlation between V, O, and Na, based on face-scanning EDS analysis, which, in

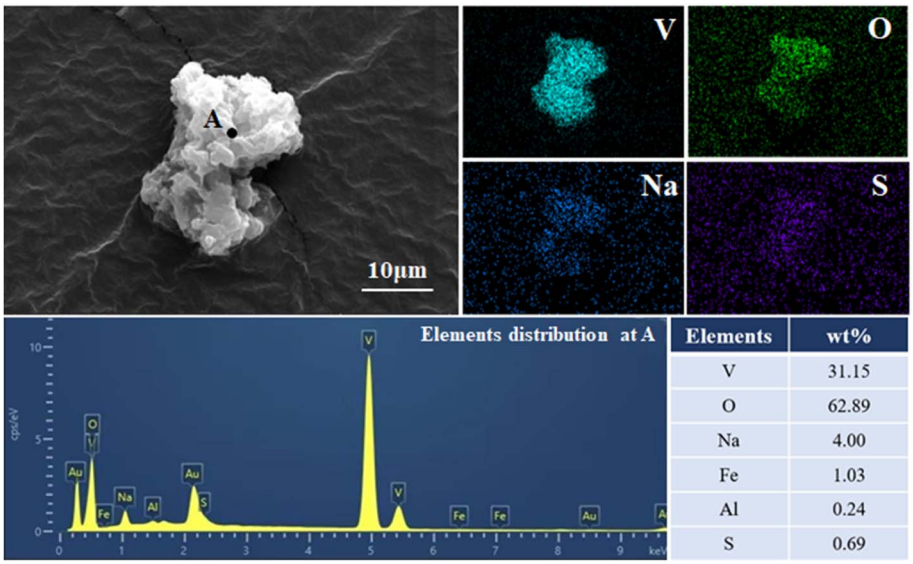

Elements	wt%
V	31.15
O	62.89
Na	4.00
Fe	1.03
Al	0.24
S	0.69

Fig. 13 ESEM micrographs with EDS element mapping of hydrolysis vanadium precipitation product.

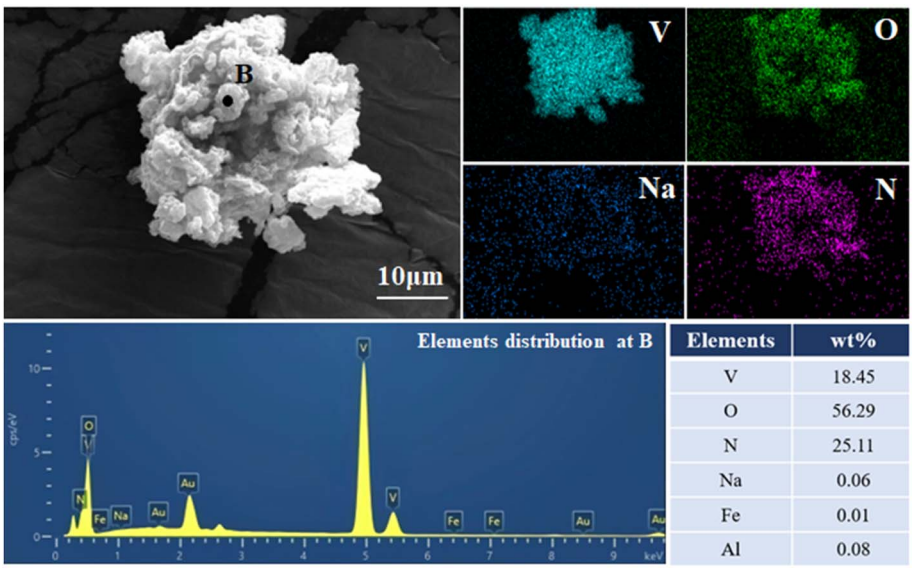

Elements	wt%
V	18.45
O	56.29
N	25.11
Na	0.06
Fe	0.01
Al	0.08

Fig. 14 ESEM micrographs with EDS element mapping of ammonium salt purification product.

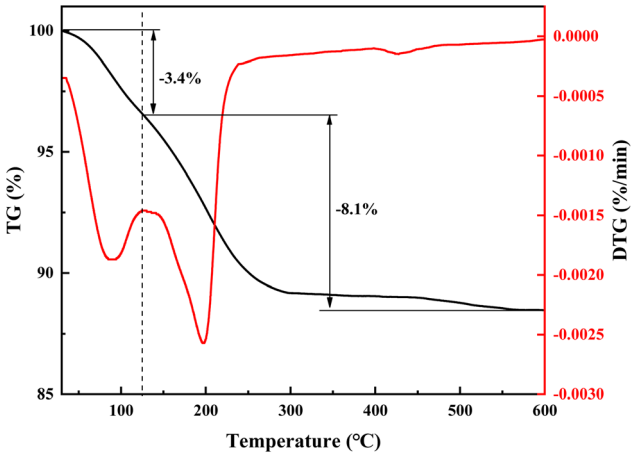

Fig. 15 TG and DTG analysis of hydrolysis vanadium precipitation products under a nitrogen atmosphere.

conjunction with the XRD results, indicates that its primary component is $NaV_3O_8 \cdot xH_2O$. In contrast, Fig. 14 shows that the ammonium salt purification product exhibits a strong correlation between V, O, and N, with a lower correlation between V and Na compared to the hydrolysis vanadium precipitation product. This supports the XRD results, suggesting that the ammonium salt purification process has effectively substituted Na^+ with NH_4^+, resulting in the formation of the new $(NH_4)_2V_6O_{16} \cdot 1.5H_2O$ phase. Additionally, it is hypothesized that nitrogen from $(NH_4)_2V_6O_{16} \cdot 1.5H_2O$ may be released as gas during the purification process, further enhancing the purity of the final V_2O_5 product.

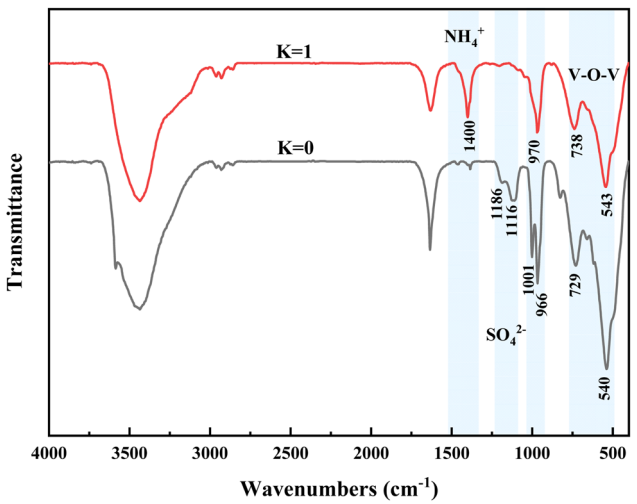

Fig. 16 FTIR spectra of hydrolysis vanadium precipitation product ($K = 0$) and ammonium salt purification product ($K = 1$).

Thermogravimetric (TG) and derivative thermogravimetry (DTG) analyses were conducted to determine the crystal water content in $NaV_3O_8 \cdot xH_2O$, the primary component of the hydrolysis vanadium precipitation product. Fig. 15 illustrates the weight loss profile of the hydrolysis vanadium precipitation product, which can be divided into two stages. The first stage, between 0 °C and 125 °C, exhibits a 3.4% weight loss, indicating the evaporation of adsorbed water. The second stage, between 125 °C and 600 °C, shows an 8.1% weight loss, corresponding to the evaporation of crystal water. Based on the weight loss observed in the second stage, the crystal water content in $NaV_3O_8 \cdot xH_2O$ can be calculated, confirming the chemical formula of sodium polyvanadate as $NaV_3O_8 \cdot 1.5H_2O$.

To further elucidate the mechanism of the ammonium salt purification process, FTIR spectroscopy was performed on both the hydrolysis vanadium precipitation and ammonium salt purification products. Fig. 16 shows that the peaks at 540 cm^{-1} and 729 cm^{-1} in the FTIR spectrum of the hydrolysis vanadium precipitation product correspond to V–O–V stretching vibrations. In contrast, the peaks at 543 cm^{-1} and 738 cm^{-1} in the FTIR spectrum of the ammonium salt purification product correspond to V–O–V bending vibrations.[37] This shift from lower to higher wavenumbers after ammonium salt purification suggests a change in the crystal structure of the hydrolysis vanadium precipitation product. Additionally, the V=O peaks at 966 cm^{-1} and 1001 cm^{-1} in the hydrolysis vanadium precipitation product disappear after purification, while a new V–O–V peak appears at 970 cm^{-1}, indicating the formation of a $V_6O_{16}^{2-}$ layers by combining two $V_3O_8^-$ layers. The peaks at 1116 cm^{-1} and 1186 cm^{-1}, which are characteristic of SO_4^{2-}, vanish in the ammonium salt purification product, while a peak at 1400 cm^{-1} corresponding to NH_4^+ bending vibrations appears. This suggests that SO_4^{2-} is leached from the solid product into the liquid phase, and NH_4^+ ions enter the solid phase during the ammonium salt purification process.

3.3. Characterization of V_2O_5 products

Vanadium precipitation at an initial pH of 1.8, a reaction time of 1.5 hours, and a temperature of 95 °C achieved a vanadium precipitation rate of 99.13%. With an ammonium addition coefficient of 1, a purification temperature of 55 °C, a purification time of 15 min, and a purification frequency of 2, the purity of V_2O_5 products exceeded 99.9%. Table 3 presents the ICP detection results for the V_2O_5 products, which exhibit a low impurity level, meeting the requirements of the V_2O_5 99.8-P grade as specified in the YB/T 5304-2017 standard. Fig. 17 shows the XRD spectrum of the V_2O_5 product, which confirms that its

Table 3 Composition of V_2O_5 products (wt%)

	V_2O_5	Fe	P	S	Al	$K_2O + Na_2O$
V_2O_5 products	99.9	0.0084	0.016	0.010	0.001	0.022
Standard sample	≥99.8	≤0.03	≤0.02	≤0.03	—	≤0.1

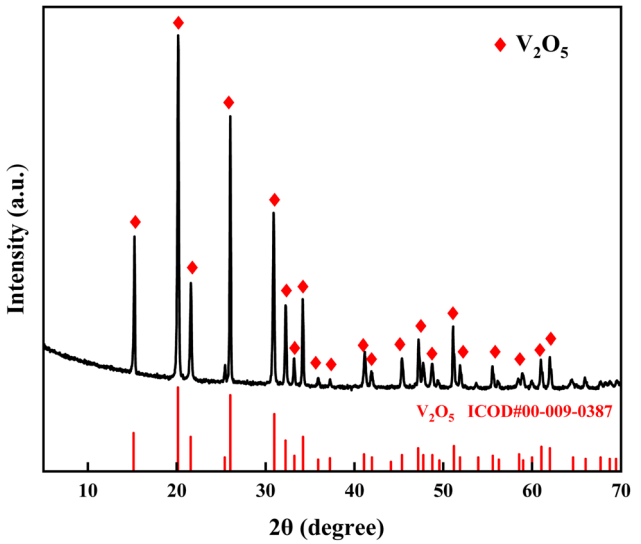

Fig. 17 XRD pattern of V_2O_5 products.

main composition is V_2O_5, with virtually no impurity peaks, supporting the high purity observed in the ICP results. Thus, high-purity V_2O_5 can be efficiently produced using the hydrolysis vanadium precipitation-ammonium salt purification process with reduced ammonium usage.

4. Conclusion

This study investigates the preparation of high-purity V_2O_5 using a D2EHPA saponification extraction-hydrolysis vanadium precipitation-ammonium salt purification process, utilizing vanadium-rich liquids with high impurity content as the raw material. The following conclusions can be drawn:

(1) The D2EPHA saponification extraction process effectively eliminates impurities from the vanadium-rich liquid. The vanadium extraction rate reached 99% after three-stage counter-current extraction under the following conditions: 60% saponification degree of D2EHPA, an initial pH of 1.8, a D2EHPA concentration of 40 vol%, a phase ratio (O/A) of 2 : 1, and an extraction time of 8 minutes. After three-stage counter-current stripping, the vanadium stripping rate achieved 99.8% under a phase ratio (O/A) of 2 : 1, an H_2SO_4 concentration of 2 mol L^{-1}, and a stripping time of 20 minutes. The concentrations of Vanadium, Fe^{2+}, and Al^{3+} in the stripping solution were 53.57 g L^{-1}, 0.034 g L^{-1}, and 0.439 g L^{-1}, respectively, with Fe^{2+} and Al^{3+} elimination rates of 98.78% and 97.93%. These results demonstrate the effectiveness of the purification and decontamination processes.

(2) The hydrolysis vanadium precipitation-ammonium salt purification process resulted in high-purity V_2O_5. The vanadium precipitation rate reached 99.13% under the optimal conditions of pH 1.8, a reaction time of 1.5 hours, and a temperature of 95 °C. The purity of the V_2O_5 products exceeded 99.9% under the following conditions: ammonium coefficient of 1, temperature of 55 °C, time of 15 minutes, and purification frequency of 2. Compared to the ammonium salt vanadium precipitation process, this method reduced the ammonium addition coefficient from 6 to 1, resulting in an 83% reduction in ammonium consumption. This makes the process more environmentally friendly while achieving high-purity V_2O_5.

(3) The D2EHPA saponification extraction process replaced H^+ in the O–H group with Na^+, facilitating Na and V substitution during the extraction process. This resulted in a pH shift and an increased vanadium extraction rate. During the ammonium salt purification process, vanadate preferentially interacts with NH_4^+ over Na^+, leading to the substitution of Na^+ with NH_4^+ in the $V_3O_8^-$ layer. This substitution disrupts the interaction between Na^+ and $V_3O_8^-$, and NH_4^+ induces a structural transformation in the $V_3O_8^-$ layer, converting the V=O bond into V–O–V. This promotes polymerization of the $V_3O_8^-$ layer into $V_6O_{16}^{2-}$layer, eventually forming $(NH_4)_2V_6O_{16} \cdot 1.5H_2O$.

Data availability

All data included in this study are available from the corresponding author upon request.

Conflicts of interest

The authors declare that they have no known competing financial interests or personal relationships that could have appeared to influence the work reported in this paper.

Acknowledgements

The authors gratefully acknowledge the financial support provided by the Science and Technology Innovation Talent Program of Hubei Province (2022EJD002) and Hubei Provincial Natural Science Foundation of China (2024AFB817).

References

1 B. Chen, S. Bao and Y. Zhang, Synergetic strengthening mechanism of ultrasound combined with calcium fluoride towards vanadium extraction from low-grade vanadium-bearing shale, *Int. J. Min. Sci. Technol.*, 2021, **31**, 1095–1106, DOI: 10.1016/j.ijmst.2021.07.008.

2 Y. Zhang, S. Bao and T. Liu, The technology of extracting of vanadium from stone coal in China: history, current status and future prospects, *Hydrometallurgy*, 2011, **109**, 116–124, DOI: 10.1016/j.hydromet.2011.06.002.

3 M. Petranikova, A. H. Tkaczyk, A. Bartl, A. Amato, V. Lapkovskis and C. Tunsu, Vanadium sustainability in the context of innovative recycling and sourcing, *Waste Manage.*, 2020, **113**, 521–544, DOI: 10.1016/j.wasman.2020.04.007.

4 S. H. Kim, E. R. Baek and B. K. Jang, The effect of vanadium addition on the fracture and wear resistance of indefinite chilled cast iron, *Mater. Today Commun.*, 2021, **26**, 101819, DOI: 10.1016/j.mtcomm.2020.101819.

5 T. Liu, G. Zhang, Y. Zhang, J. Huang, Z. Fu and Q. Shi, Recycle of vanadium precipitated liquor in extraction of

vanadium from stone coal, *Chin. J. Rare Met.*, 2016, **40**, 85–91, DOI: 10.13373/j.cnki.cjrm.2016.01.014.

6 E. D. Carpio, L. Hernandez, C. Ciangherotti, V. V. Coa, L. Jimenez, V. Lubes and G. Lubes, Vanadium: History, chemistry, interactions with a-amino acids and potential therapeutic applications, *Coord. Chem. Rev.*, 2018, **372**, 117–140, DOI: 10.1016/j.ccr.2018.06.002.

7 A. Norah, Investigation on structural, optical, thermal, and dielectric properties of nanocomposite films based on chitosan containing vanadium pentoxide/zinc oxide and their potential for optoelectronics devices, *J. Mol. Struct.*, 2024, **1312**, 138491, DOI: 10.1016/j.molstruc.2024.138491.

8 N. Beriwal and A. Verma, Development of economical and highly efficient electrolyte using vanadium pentoxide for vanadium redox flow battery, *Environ. Sci. Pollut. Res.*, 2022, **29**, 72187–72195, DOI: 10.1007/s11356-021-18367-5.

9 C. Wu and Y. Xie, Promising vanadium oxide and hydroxide nanostructures: from energy storage to energy saving, *Energy Environ. Sci.*, 2010, **3**, 1191–1206, DOI: 10.1039/c0ee00026d.

10 P. Hu, Y. Zhang, J. Huang, T. Liu, Y. Yuan and N. Xue, Eco-friendly leaching and separation of vanadium over iron impurity from vanadium-bearing shale using oxalic acid as a leachate, *ACS Sustainable Chem. Eng.*, 2018, **6**, 1900–1908. https://www.x-mol.com/paperRedirect/469538.

11 Y. Zhang, D. Dreisinger, T. Zhang, G. Lv, W. Zhang and F. Xie, Preparation of highly pure vanadyl sulfate electrolyte from vanadium slag leach solution with the complexing effect of EDTA on Fe (III), *Hydrometallurgy*, 2019, **188**, 54–63, DOI: 10.1016/j.hydromet.2019.05.012.

12 Y. An, B. Ma, Z. Zhou, Y. Chen, C. Wang, B. Wang, M. Gao and G. Feng, Extraction of vanadium from vanadium slag by sodium roasting-ammonium sulfate leaching and removal of impurities from weakly alkaline leach solution, *J. Environ. Chem. Eng.*, 2023, **11**, 110458, DOI: 10.1016/j.jece.2023.110458.

13 B. Chen, S. Bao and Y. Zhang, Effects of key impurities (Al, Fe, P, Si and Na) on the precipitation process of vanadium in the novel ultrasound-assisted precipitation system, *Hydrometallurgy*, 2024, **224**, 106233, DOI: 10.1016/j.hydromet.2023.106233.

14 C. Chen, H. Zuo and H. Wang, Study on the preparation technology of high-purity V_2O_5, *World Nonferrous Metals*, 2019, **2**, 206–208.

15 K. Kurniawan, H. Leeb, M. Baeb, J. W. Choib and S. Kima, Intensified extraction of vanadium from vanadium-bearing titanomagnetite (VTM) concentrate *via* one-stage leaching and solvent extraction using acidic organophosphorus extractant, *Miner. Eng.*, 2024, **217**, 108961, DOI: 10.1016/j.mineng.2024.108961.

16 Z. Liu, J. Huang, Y. Zhang, T. Liu, P. Hu, H. Liu and D. Luo, Separation and recovery of vanadium and aluminum from oxalic acid leachate of shale by solvent extraction with Aliquat 336, *Sep. Purif. Technol.*, 2020, **249**, 116867, DOI: 10.1016/j.seppur.2020.116867.

17 W. Li, Y. Zhang, T. Liu, J. Huang and Y. Wang, Comparison of ion exchange and solvent extraction in recovering vanadium from sulfuric acid leach solutions of stone coal, *Hydrometallurgy*, 2013, **131–132**, 1–7, DOI: 10.1016/i.hydromet.2012.09.009.

18 Z. Ying, Y. Song, K. Zhu, G. Wu, Y. Ju, Q. Wei and X. Ren, A cleaner and sustainable method to recover vanadium and chromium from the leaching solution based on solvent extraction, *J. Environ. Chem. Eng.*, 2022, **10**, 107384, DOI: 10.1016/j.jece.2022.107384.

19 H. Wang, Y. Feng, H. Li, H. Li and H. Wu, Recovery of vanadium from acid leaching solutions of spent oil hydrotreating catalyst using solvent extraction with D2EHPA (P204), *Hydrometallurgy*, 2020, **195**, 105404, DOI: 10.1016/j.hydromet.2020.105404.

20 H. Liu, Y. Zhang, T. Liu, J. Huang, L. Chen and Y. Hu, Preparation of vanadium electrolyte from vanadium shale leaching solution with high concentration chloride using D2EHPA, *Trans. Nonferrous Met. Soc. China*, 2023, **33**, 1594–1608, DOI: 10.1016/S1003-6326(23)66206-5.

21 M. Sun, S. Liu, Y. Zhang, M. Liu, X. Yi and J. Hu, Insights into the saponification process of di(2-ethylhexyl) phosphoric acid extractant: Thermodynamics and structural aspects, *J. Mol. Liq.*, 2019, **280**, 252–258, DOI: 10.1016/j.molliq.2019.02.025.

22 G. Zhang, Y. Zhang, S. Bao and L. Zhang, A novel process for the synthesis of NaV_2O_5 mesocrystals from alkaline-stripped vanadium solution via the hydrothermal hydrogen reduction method, *Minerals*, 2019, **9**(5), 271, DOI: 10.3390/min9050271.

23 L. Liu, T. Kauppinen, P. Tynjal, T. Hu and U. Lassi, Water leaching of roasted vanadium slag: desiliconization and precipitation of ammonium vanadate from vanadium solution, *Hydrometallurgy*, 2023, **215**, 105989, DOI: 10.1016/j.hydromet.2022.105989.

24 S. Zhou, M. Dong, X. Ding, X. Xue and H. Yang, Application of RSM to optimize the recovery of ammonia nitrogen from high chromium effluent produced in vanadium industry using struvite precipitation, *J. Environ. Chem. Eng.*, 2021, **9**, 106318, DOI: 10.1016/j.jece.2021.106318.

25 S. Wang, X. Guo, H. Du, S. Zheng, B. Liu and Y. Zhang, Solubility investigations in the $(NH_4)_2C_2O_4$-NH_4VO_3-H_2O system from 313.15 to 363.15K, *J. Chem. Eng. Data*, 2017, **62**, 3313–3318, DOI: 10.1021/acs.jced.7b00362.

26 X. Yang, Y. Zhang and S. Bao, Preparation of high purity V_2O_5 from a typical low grade refractory stone coal using a pyro-hydrometallurgical process, *Minerals*, 2016, **6**(3), 69, DOI: 10.3390/min6030069.

27 J. Song, Z. Gao, H. Su, H. Shi and C. Zhu, Exploration of process optimization for recovery of sodium and ammonium sulfate crystals from vanadium precipitation wastewater, *J. Cryst. Growth*, 2022, **598**, 126872, DOI: 10.1016/j.jcrysgro.2022.126872.

28 S. Zhou, M. Dong, X. Ding, X. Xue, H. Yang and X. Zhang, A near-zero-waste approach using simple physical-chemical methods recovery high concentrations of ammonia nitrogen, heavy metal, and sodium salts from hazardous vanadium-extracted solution, *J. Cleaner Prod.*, 2021, **316**, 128363, DOI: 10.1016/j.jclepro.2021.128363.

29 H. Peng, J. Guo, B. Li and H. Huang, Vanadium properties, toxicity, mineral sources and extraction methods: a review, *Environ. Chem. Lett.*, 2022, **20**, 1249–1263, DOI: **10.1007/s10311-021-01380-y**.

30 Z. Wu and L. Jiang, Study on Vanadium Precipitation by Hydrolysis of Chromium-vanadium Solution, *Iron, Steel, Vanadium, Titanium*, 2020, **41**(5), 22–26, DOI: **10.7513/j.issn.1004-7638.2020.05.004**.

31 Z. Fu, Y. Zhang, T. Liu, J. Huang and X. Yang, Impact of impurity ions on vanadium precipitation process of stripping solution from vanadium extraction of stone coal, *Chin. J. Rare Met.*, 2016, **40**(10), 1060–1065, DOI: **10.13373/j.cnki.cjrm.xy15032601**.

32 G. Lin, J. Huang, Y. Zhang and P. Hu, A Sustainable Technique to prepare high-purity vanadium pentoxide via purification with low ammonium consumption, *Materials*, 2022, **15**(5), 1945, DOI: **10.3390/ma15051945**.

33 M. Sun, S. Liu, Y. Zhang, M. Liu, X. Yi and J. Hu, Insights into the saponification process of di(2-ethylhexyl) phosphoric acid extractant: Thermodynamics and structural aspects, *J. Mol. Liq.*, 2019, **280**, 252–258, DOI: **10.1016/j.molliq.2019.02.025**.

34 B. Han, J. Li, J. Zhong, S. Li, S. Yang, Y. Chen and H. Zhang, Research progress of acid organic phosphorus extractants in extraction of valuable metals, *J. Cent. South Univ. (Sci. Technol.)*, 2023, **54**(9), 3402–3420, DOI: **10.11817/j.issn.1672-7207.2023.09.003**.

35 Y. Hu, Y. Zhang, T. Liu and H. Liu, Clean and cost-efficient preparation of vanadium electrolyte from the vanadium-rich solution of black shale by solvent extraction, *J. Cleaner Prod.*, 2023, **394**, 136389, DOI: **10.1016/j.jclepro.2023.136389**.

36 H. Liu, Y. Zhang, T. Liu, J. Huang and Q. Shi, Optimization Study on Vanadium Extraction Process by Saponified P204, *Nonferrous Metals (Extractive Metallurgy)*, 2016, issue 05, pp. 17–21, DOI: **10.3969/j.issn.1007-7545.2016.05.005**.

37 S. Ullah, W. Shahid, S. Shahid, M. I. Khan, N. Ansar, M. Khizar, S. Ali, J. R. Choi, B. S. Almutairi and M. A. Alreshidi, Advancing photocatalysis: Innovative approaches using novel V2O5/ZnO nanocomposites for efficient photocatalytic degradation of tubantin red, *J. Saudi Chem. Soc.*, 2023, **27**, 101766, DOI: **10.1016/j.jscs.2023.101766**.